Synthesis, Microstructure, Photocatalytic and Antibacterial Properties of ZnO-ZrO_2 Nanocomposite

Jingjun YUAN *, Xin YAO

Wuxi Zhong Wei-High-tech Electronics Co. Ltd, Wuxi 214000, Jiangsu, China

http://doi.org/10.5755/j02.ms.38437

Received 12 August 2024; accepted 4 November 2024

Zinc oxide -Zirconium oxide (ZnO-ZrO_2) nanocomposite (NC) was prepared using a sol-gel process. X-ray diffraction (XRD) studies showed the tetragonal and hexagonal structures of ZrO_2 and ZnO respectively. FTIR studies indicated the Zn-O and Zr-O bonds in the prepared sample. The electron microscopy analysis showed the presence of crystalline materials with a uniform and compact structure. The optical studies showed a sharp absorption at about 400 nm and the Tauc plot evaluated the bandgap of 3.15 eV. The photodegradation performance of Methylene Blue (MB) dye was obtained for ZnO-ZrO_2 NC using visible light irradiation and showed 96.89 % efficiency. The antibacterial activity of ZnO-ZrO_2 NC against certain bacteria was investigated and the results indicated the significant antibacterial activity.
Keywords: zirconium oxide, zinc oxide, microstructure, antibacterial, photocatalytic activity, nanocomposite.

1. INTRODUCTION

ZnO-ZrO_2 nanocomposite refers to nanoparticles composed of a combination of zinc oxide (ZnO) and zirconium dioxide (ZrO_2). This nanocomposite holds significance in different areas because of its unique properties and potential applications. ZnO is a wide bandgap semiconductor material with excellent optical, electrical, and photocatalytic properties [1 – 3]. ZrO_2, also known as zirconia, is an n-type semiconductor material with high thermal stability, chemically inert with hardness. ZrO_2 exists in different phases based on its temperature. ZrO_2 is a wide bandgap material, whose bandgap lies between 5.0 – 5.5 eV and hence it requires UV light for excitation and charge carriers production. ZrO_2 is doped with various metal ions or coupled with other metal oxides to counteract the use of UV light. The composites of two metal oxides have shown enhanced physico-chemical properties as compared to the pure oxides. Typically, composites improve the efficiency of photocatalytic activity [4]. Composites consisting of ZrO_2 and ZnO have recently gained significant interest due to their outstanding characteristics as a semiconductor material. The combination of ZnO and ZrO_2, resulting synergistic effects, where the properties of the composite material are superior to the individual materials. The improved degradation activity of ZnO-ZrO_2 relates to modifications in its structure, orientation, and optical properties [5 – 7]. The unique properties of ZnO-ZrO_2 make them promising candidates for gas sensors, biosensors, and chemical sensors. ZnO-ZrO_2 NC has potential applications in bioimaging, drug delivery, and tissue engineering due to its biocompatibility and controlled release properties.

Furthermore, the enhanced electron-hole pair amplifies photocatalytic activity. When exposed to light, both semiconductors in the NC become excited at the same time. ZnO-ZrO_2 NC can be used in photocatalytic applications for environmental remediation, such as water purification and air treatment, due to their ability to degrade organic pollutants under illumination [7].

Bacterial toxicities are a significant contributor to the occurrence of long-lasting infections and death. Antibiotics were the favoured therapeutic approach for bacterial infections due to their cost effectiveness and potent efficacy [8]. Nevertheless, numerous studies have presented conclusive evidence that the extensive utilization of antibiotics, resulting in the creation of bacterial strains that are resistant to multiple drugs. In recent times, the improper use of antibiotics has resulted in the creation of super-bacteria that exhibit a high level of resistance to nearly all antibiotics [9,10]. There has been a shift in focus towards novel and stimulating materials based on nanoparticles (NPs) that possess antibacterial properties.

Aghabeygi et al [11] synthesized ZrO_2: ZnO as a catalyst for the degradation of CR dye and suggested that ZnO has the potential to increase the abundance of unbound electrons in the conduction band of ZrO_2 by minimizing the occurrence of charge recombination during electron transportation. Uribe López et al [12] synthesized ZnO-ZrO_2 NC and used it for photodegradation of phenol and found good degradation efficiency. Gurushantha et al. [13] revealed the improved photocatalytic activity for the orange 8 dye when exposed to UV light for ZrO_2-ZnO NC. The researchers noted a decrease in the bandgap, an increase in the density of states, and an improvement in the stability of the composite, resulting in enhanced efficiency of the photocatalyst.

Ayodeji and Simón [14] prepared the pure ZrO_2, ZnO, and ZrO_2−ZnO NPs and studied the antibacterial activity. Various methods can be employed to synthesize ZnO-ZrO_2 NPs, including sol-gel, hydrothermal synthesis, chemical vapour deposition, and co-precipitation techniques. The optimum synthesis method can influence the microstructure and properties of the nanoparticles. The sol-gel process was used in this work due to its simple and cost

* Corresponding author: J. Yuan
E-mail: *yuanjingjun@cetcpkg.com*

effective. In this work, the ZnO-ZrO_2 NPs are prepared, and microstructural, optical, photocatalytic, and antibacterial activities were investigated.

2. MATERIALS AND METHODS

2.1. Materials

The chemicals employed in this investigation were AR grade and used without further process. The experiment utilised deionized (DI) water only. 4.6246 g of Zirconium nitrate ($Zr(NO_3)$ $3(H_2O)$**)** and 3.6696 g of zinc acetate dihydrate ($Zn(CH_3COO)_2$ $2(H_2O)$ was dissolved in DI water separately and the first solution was added to the later one. Later, CTAB was added as a surfactant. 2.1014 g of citric acid was dissolved as the gelling agent. The solution was kept at about 70 – 80 °C and calcined at 600 °C for 2 h.

2.2. Determination of antibacterial activity

Penicillin was used as a control drug. The antibacterial activity was studied using the standard diffusion disc plates on agar, whereas the MIC was obtained using the dilution method. The pure cultures of organisms (E. coli (ATCC15224), Salmonella typhimurium (ATCC13048), Bacillus cereus (ATCC13061), Shigella flexneri (ATCC12022), Pseudomonas aeruginosa (ATCC6643) were sub-cultured in nutrient broth.

A minimum of 3 – 5 distinct colonies, displaying the same physical characteristics, were chosen from a culture of a specific microbe grown on an agar plate.

Mueller-Hinton Agar is widely regarded as the optimal choice for routine susceptibility testing of non-fastidious bacteria due to several key advantages [15].

2.3. Photocatalytic studies

The photocatalytic performance of the sample was measured using the MB dye solution of 10 ppm. The solution was kept in a dark environment for 30 min to attain an equilibrium state. The solution was exposed to visible light (550 nm) light and 2 mL solution was taken at 30 min time intervals. The UV-vis spectrophotometer was employed to analyse the absorption of the sample.

2.4. Characterization details

The sample's structure was studied using an X-ray diffractometer (XRD) with CuKα radiation (Rigaku, Ultima IV). FTIR spectrometer (Jasco 4200 model) was utilized for the analysis of bond vibrations in a sample. The FESEM was used for the analysis of surface morphology (Quanta FEG-250). The optical studies of the sample were analysed using UV-Visible spectrophotometer (Shimadzu) in the 200 – 1000 nm region.

3. RESULTS AND DISCUSSION

3.1. Microstructural studies

XRD technique was used to investigate the structure of the sample ZnO–ZrO_2 NC. XRD pattern shows the sharp peaks at 31.70°, 34.20°, 36.30°, 47.6°, 56.6°, 63.0°, 66.3°, 67.9°, 69.0° that correspond to (100), (002), (101), (102), (110), (103), (200), (112), (201), reflections and in agreement with the ZnO hexagonal phase (JCPDS 36-1451) (Fig. 1). The strong intensity of the (101) reflection indicates the presence of anisotropic development and orientation of the crystals [16, 17]. The peaks also located at 26.1, 28.30°, 30.40°, 50.4°, 60.0° and 74.5° correspond to m (-110), m (-111), t (111), t (202), t (311), and t (400) planes indicating the monoclinic (m) and tetragonal (t) phases of ZrO_2 (JCPDS Nos. 79-1771 and 37-1484). The results indicate both tetragonal and monoclinic structures present in the sample with the predominant tetragonal phase [16 – 19]. The Scherer equation was used to compute the crystallite size:

$$D = \frac{K\lambda}{\beta \cos\theta}, \quad (1)$$

where K is the Sherrer constant (0.9); λ is the incident X-ray wavelength; β is the full width at half maximum; θ is diffraction angle.

No other impurities were found in the sample. The crystallite sizes of ZrO_2 and ZnO were determined using the Scherer equation, yielding values of 18 nm and 19 nm, respectively.

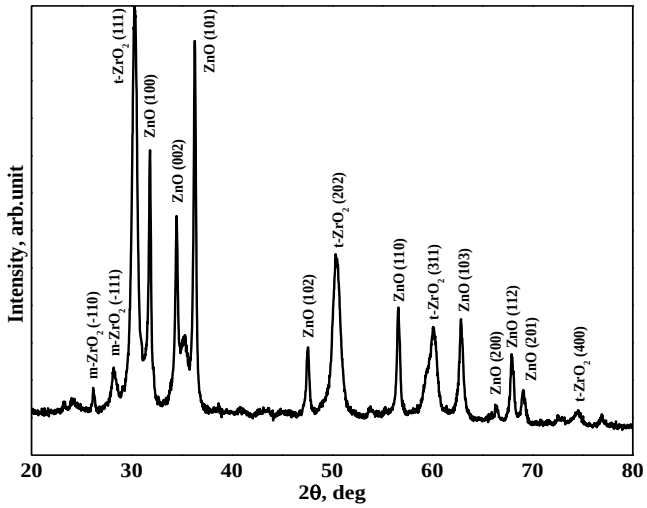

Fig. 1. XRD pattern of ZnO-ZrO_2 nanocomposite

S. Aghabeygi and M. Khademi-Shamami synthesized the ZnO-ZrO_2 NC using a sol-gel method with different molar ratios. XRD results showed a monoclinic phase of ZrO_2 and ZnO hexagonal structure [5]. Uribe López et al synthesized ZnO-ZrO_2 NC using a sol-gel process and the XRD results revealed the tetragonal structure for ZrO_2 and ZnO of hexagonal structure [12]. S. Aghabeygi et al. synthesized the ZnO NPs and ZrO_2/ZnO NCs using the sol-gel technique. XRD studies showed the presence of a hexagonal phase in ZnO and a monoclinic structure of ZrO_2 [11]. Mohammed Tuama et al. [20] green synthesized and characterized ZnO: ZrO_2 sample and the XRD shows the hexagonal phase of ZnO and ZrO_2 is a monoclinic and a tetragonal structure.

FTIR spectrum of the sample is shown in Fig. 2. The peak seen ~ 3668 cm^{-1} corresponds to the stretching vibrations of H_2O and M–O–H bonds, specifically related to the symmetry and asymmetry of the OH groups. The peaks ~ 1580 cm^{-1} belong to the bending vibration of the adsorbed H_2O, which has not been eliminated following the sol-gel manufacturing process. The peak at around

1250 cm^{-1} is associated with the bending vibrations of surface M–O–H bonds.

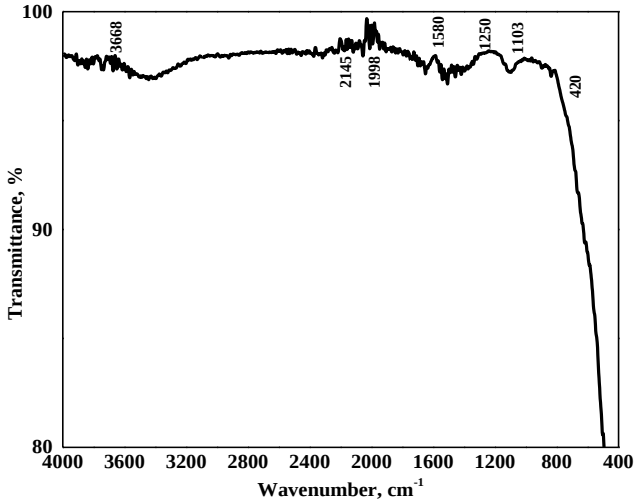

Fig. 2. FTIR spectrum of the ZnO/ZrO_2 NC

The peaks ~ 420 and 500 cm^{-1} are due to the bending vibrations of Zn–O–Zn chemical bonds. The peaks detected at 700 cm^{-1} and 800 cm^{-1} correspond to the oscillation of Zn–O–Zr and the symmetrical and asymmetrical stretching oscillations of O–Zr–O bonds, respectively.

S. Aghabeygi et al. prepared the $ZnO–ZrO_2$ NPs via sol-gel method and used FTIR studies to analyse the structural characteristics of the ample. The FTIR spectrum displays the vibrational modes of Zn–O at 566 and 659 cm^{-1}, the surface O–H bending vibration at 1365 cm^{-1}, the bending vibration of water at 1608 cm^{-1}, and the stretching vibration of water at 3451 cm^{-1}. The vibrations seen at 802 cm^{-1} belong to the Zr–O bond. FTIR studies confirmed that ZnO and ZrO_2 NPs in the clay structures and agree with other reported results [5, 11, 12].

The surface topography of the synthesized NPs was analyzed using FESEM. Fig. 3 shows the NPs are in uniform size, and dense structure with smooth morphology. The NPs are aggregated and agglomerated. The EDX analysis confirmed the Zn, Zr, and O elements present in the sample and there are no other impurities found in the sample. This indicates the successful doping of ZrO_2 into the ZnO matrix [5, 11, 12].

3.2. Optical properties

The UV-Visible spectrophotometer was employed to investigate the optical properties of the sample. Fig. 4 shows the absorption spectrum of the $ZnO–ZrO_2$ sample. The absorption phenomena, linked to the electrical transition from the valence band to the conduction band, was utilised to determine the properties and extent of the bandgap (*Eg*). A sharp absorption was found about 400 nm, indicating the transition from VB to CB. The bandgap can be obtained using the Tauc plot. The Eq. 2 is used to find the bandgap of the sample:

$$(\alpha h\nu)^2 = A\,(h\nu - Eg), \quad (2)$$

where α is the absorption coefficient; ν is the frequency of radiation; *Eg* is the bandgap.

The bandgap of the sample was computed using the Tauc plot; $(\alpha h\nu)^2$ and $h\nu$ at $\alpha = 0$. (Fig. 4). The calculated bandgap of the $ZnO–ZrO_2$ sample was 3.15 electronvolts (eV).

Shokufeh Aghabeygi et al. prepared the $ZnO–ZrO_2$ by sol gel process at different molar ratios. UV-vis absorption spectra showed the absorption peaks and the calculated *Eg* values were 5.38 eV, 4.31 eV, and 4.85 eV for 2:1, 1:2 and 1:1 molar ratio respectively [5]. $ZnO–ZrO_2$ NCs were prepared through the sol-gel method with different ZnO ratios.

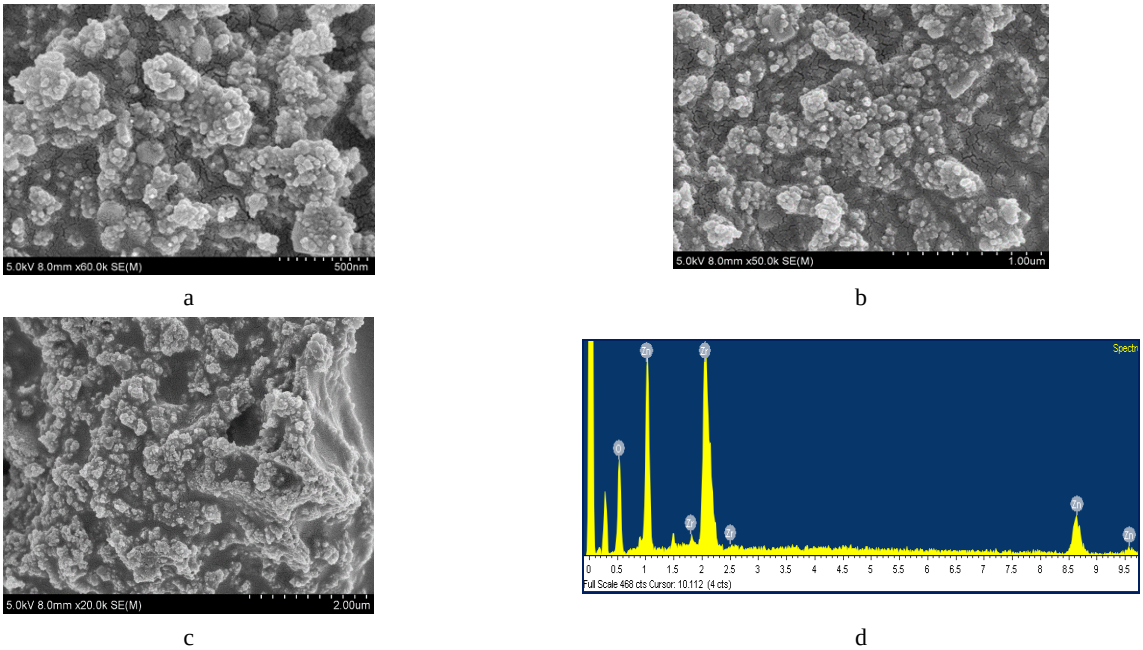

Fig. 3. a, b, c – FESEM images; d – EDX analysis of the ZnO/ZrO_2 NC

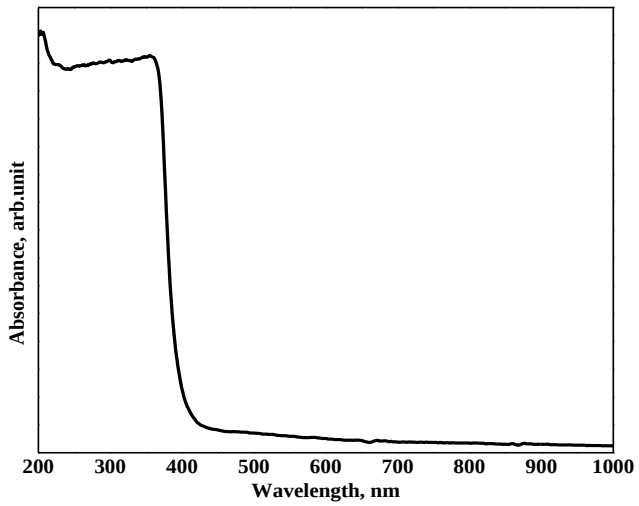

a

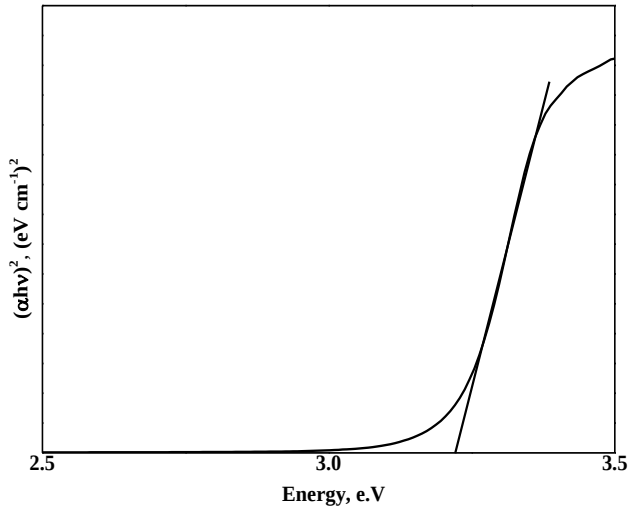

b

Fig. 4. UV–visible spectroscopy of the ZnO-ZrO_2 sample: a – absorption spectrum; b – Tauc plot

The bandgap values were 3.07 – 3.16 eV range for the composites and excited at lower energy [12]. In the present work, the bandgap is found to be 3.15 eV and the value is similar to other reported values. The optical studies showed a bandgap of 3.15 eV and 4.6 eV for the ZnO and ZrO_2 samples, respectively [20].

3.3. Photocatalytic studies

Textile businesses typically employ dyes with intricate structures that make them very resistant to degradation caused by environmental factors. As a result, the traditional methods for treating wastewater continue to be ineffectual. Currently, adsorption is the primary commercially feasible method for treating dye wastewater. Fig. 5 demonstrates the degradation of Methylene Blue (MB) dye through photodegradation using ZnO–ZrO_2 NC under visible light exposure. The absorbance reached a minimum and the MB dye solution became colourless after 2 h at visible light exposure. The absorbance diminished because of the dyes' degradation in the presence of nanoparticles (catalyst). The bandgap is 3.15 eV for ZnO and ZrO_2 NC and hence when the electrons are excited, electrons from Conduction Band (CB) (ZrO_2) easily reach the CB (ZnO) and the bandgap is decreased, indicating the ZnO-ZrO_2 NC has a suitable bandgap to generate e- and h+ pairs and allowing the use of visible light for photocatalytic activity. This material exhibits a bandgap of 3.15 eV, which enables it to efficiently absorb visible light. The degree of MB photodegradation can be calculated using the method [21].

$$\text{Degradation} = [A0\text{-}At/A0]\times 100, \quad (3)$$

where *A*0 and *A*t are the initial and final absorbance values of MB, respectively. The degree of MB photodegradation was 96.89 %. The result agrees with other reported results [21 – 23].

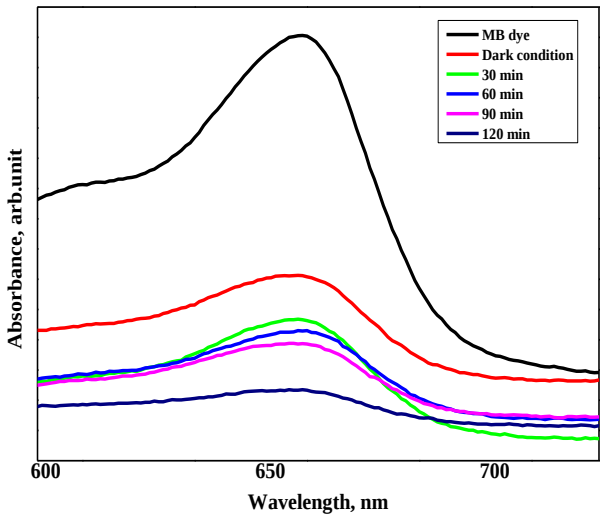

Fig. 5. Photocatalytic degradation of MB dye using ZnO–ZrO_2 catalyst

S. Aghabeygi et al. synthesized the ZrO_2–ZnO NC by sol-gel process and the photocatalytic activity results showed an efficiency of 92 % in CR dye degradation under UV light illumination [11]. Uribe López et al prepared the ZnO–ZrO_2 NCs and used them for the photocatalytic degradation of phenol and found that the 75ZnO–ZrO_2 NC revealed a higher efficiency as compared to pure ZnO [12].

3.4. Antibacterial activity

Fig. 6 represents the antibacterial potential of the control drug penicillin and ZnO–ZrO_2 NC on some selected bacterial pathogens.

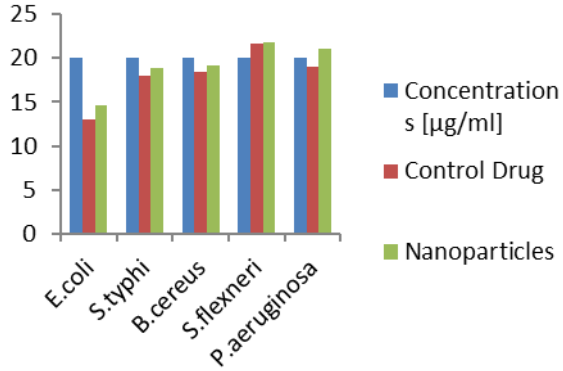

Fig. 6. MIC of penicillin and nanocomposite on selected microorganisms

This work is to study the antibacterial effects of ZnO–ZrO_2 NPs along with commercial antibiotic drug penicillin. Fig. 6 shows the minimum inhibitory concentration of 14 µg/ml in E.Coli. B. cereus and S. typhi show moderate inhibition. The NPs show significant antibacterial activity as compared to the control drug Penicillin at the concentration of 20 µg/ml. The results demonstrate that the NPs exhibit substantial efficacy against specific microorganisms.

Metallic nanoparticles have shown significant interest because of the ongoing increase in antibacterial infections and diseases, as well as the lack of effective treatment. Furthermore, the rapid increase in antibiotic resistance during this time has prompted researchers and scientists to re-examine the therapeutic properties of silver and its nanoparticulate systems as possible antimicrobial agents [8]. The agar diffusion antimicrobial test enables the assessment of the antimicrobial efficacy of various materials. However, its conclusions are limited as they are contingent upon the solubility of the item being tested. Alternative approaches for evaluating antibacterial activity involve the direct exposure of materials to free-floating microorganisms. Ayodeji and Simón [14] prepared the ZnO-ZrO_2 NPs and analysed the antibacterial activity and found good inhibition.

There are many researchers who studied the ZnO–ZrO_2 nanocomposite and analysed the photocatalytic and antibacterial activities. Mohammed Ahmed Wahba et al. [24] prepared the ZrO_2–ZnO NC by sol-gel process and found that the photocatalytic activity increased with ZrO_2 concentration. Wahba and Yakout [25] synthesized ZrO_2/ZnO by microwave method and analyzed using XRD, SEM, and diffuse reflectance spectroscopy techniques. The ZrO_2/ZnO showed the the superior sunlight catalytic activity. Abhijit et al. [26] et al prepared ZnO–ZrO_2 nanocomposite using a solution combustion process. The concentration of ZrO_2 in ZnO affected the microstructure and optical properties. The degradation efficiency is studied for different contents of ZrO_2. Olga Długosz et al. [27] prepared the ZrO_2–ZnO nanoparticles using precipitation with microwave method with different content of ZrO_2 and found that the 10 % ZrO_2 exhibited the maximum photocatalytic activity. These investigations revealed that the ZnO–ZrO_2 nanocomposite exhibited superior photodegradation and antibacterial activities.

4. CONCLUSIONS

ZnO–ZrO_2 nanocomposite was synthesized using the sol-gel method. XRD results showed both the monoclinic and tetragonal phases of ZrO_2 and the hexagonal phase of ZnO. FTIR analysis confirmed the formation of bonds present in the sample. FE-SEM analysis indicated the formation of NPs with dense and uniform structures. The optical studies revealed a bandgap of 3.15 eV. The photodegradation efficiency of ZnO–ZrO_2 NC is found to be 96.89 % for MB dye. The ZnO–ZrO_2 NC showed significant antibacterial activity as compared to the control drug penicillin.

REFERENCES

1. **Mohan, A.C., Renjanadevi, B.** Preparation of Zinc Oxide Nanoparticles and its Characterization Using Scanning Electron Microscopy (SEM) and X-ray Diffraction (XRD) *Procedia Technology* 24 2016: pp. 761 – 766. https://doi.org/10.1016/j.protcy.2016.05.078
2. **Jinjun, Z., Meng, K., Yanxin, C., Zhijiang, J.** Environment-friendly Ternary ZnO/$ZnFe_2O_4$/TiO_2 Composite Photocatalyst with Synergistic Enhanced Photocatalytic Activity under Visible-light Irradiation *Solid State Sciences* 129 2022: pp. 106913. https://doi.org/10.1016/j.solidstatesciences.2022.10693
3. **Nedra, A., Imene, B., Meilin, C., Nejib, S., Morched, C., Jun, X.** Green Synthesis and Characterization of Zinc Oxide Nanoparticles using Mulberry fruit and Their Antioxidant Activity *Materials Science (Medžiagotyra)* 28 2022: pp. 144 – 150. http://dx.doi.org/10.5755/j02.ms.28314
4. **Hussein, A.M., Shende, R.V.** Enhanced Hydrogen Generation using ZrO_2-modified Coupled ZnO/TiO_2 Nanocomposites in the absence of Noble metal Co-catalyst *International Journal of Hydrogen Energy* 39 2014: pp. 5557 – 5568. https://doi.org/10.1016/j.ijhydene.2014.01.149
5. **Aghabeygi, S., Khademi-Shamami, M.** ZnO/ZrO_2 Nanocomposite: Sonosynthesis, Characterization and its Application for Wastewater Treatment *Ultrasonics Sonochemistry* 41 2018: pp. 458 – 465. https://doi.org/10.1016/j.ultsonch.2017.09.020
6. **Ibrahim, M.M.** Photocatalytic Activity of Nanostructured ZnO–ZrO_2 Binary Oxide using Fluorometric Method *Spectrochimica Acta Part A: Molecular and Biomolecular Spectroscopy* 145 2015: pp. 487 – 492. https://doi.org/10.1016/j.saa.2015.02.057
7. **Lakshmi, G.C., Ananda, S., Somashekar, R., Ranganathaiah, C.** Synthesis of ZnO/ZrO_2 Nanocomposites by Electrochemical Method and Photocatalytic Degradation of Fast green dye, Paper dyeing and Printing press Effluent *International Journal of Advanced Materials Science* 3 2012: pp. 221 – 237. http://www.ripublication.com/ijams.htm
8. **Hsueh, P.R.** New Delhi metallo-β-lactamase-1 (NDM-1): An Emerging Threat Among Enterobacteriaceae *Journal of the Formosan Medical Association* 109 2010: pp. 685 – 687.
9. **Poole, K.** Mechanisms of Bacterial Biocide and Antibiotic Resistance *Journal of Applied Microbiology* 92 2002: pp. 55S – 64S.
10. **Jayaraman, R.** Antibiotic Resistance: An Overview of Mechanisms and a Paradigm Shift *Current Science* 96 2009: pp. 1475 – 1484. https://www.jstor.org/stable/24104776
11. **Aghabeygi, S., Modaresi-Tehrani, M., Ahmadi, S.** Enhancing the Photocatalytic Properties of ZrO_2/ZnO Nanocomposite Supported on Montmorillonite clay for Photodegradation of Congo Red *Journal of Electronic Materials* 50 2021: pp. 2870 – 2878. https://doi.org/10.1007/s11664-021-08805-y
12. **Uribe López, M.C., Alvarez Lemus, M.A., Hidalgo, M.C., López González, R., Quintana Owen, P., Oros-Ruiz, S., Uribe López, S.A., Acosta, J.** Synthesis and Characterization of ZnO-ZrO_2 Nanocomposites for Photocatalytic Degradation and Mineralization of Phenol *Journal of Nanomaterials* 2019: pp. 12. https://doi.org/10.1155/2019/1015876

13. **Gurushantha, K., Renuka, L., Anantharaju, K.S., Vidya, Y.S., Nagaswarupa, H.P., Prashanth, S.C., Naga, B**. Photocatalytic and Photoluminescence Studies of ZrO_2/ZnO Nanocomposite for LED and Waste Water Treatment Applications *Materials Today: Proceedings* 4 2017: pp. 11747 – 11755. https://doi.org/10.1016/j.matpr.2017.09.091
14. **Precious, A.A., Reyes-López, S.Y.** ZrO_2−ZnO Nanoparticles as Antibacterial Agents *ACS Omega* 4 2019: pp. 19216 – 19224. https://doi.org/10.1021/acsomega.9b02527
15. **Athirah, N.A., Palanisamy, N.K., Zaini, M.Z., Liew, J.P., Durairaj, R.** Antibacterial Effect of Silver Nanoparticles on Multi drug Resistant Pseudomonas Aeruginosa *World Academy of Science, Engineering and Technology* 6 2012: pp. 210 – 213.
16. **Ba-Abbad, M.M., Kadhum, A.A.H., Bakar Mohamad, A., Takriff, M.S., Sopian, K.** The Effect of Process Parameters on the Size of ZnO Nanoparticles Synthesized via the Sol–gel Technique *Journal of Alloys and Compounds* 550 2013: pp. 63 – 70. https://doi.org/10.1016/j.jallcom.2012.09.076
17. **Balakrishnan, G., Vivek, S., Yogesh Palai, P., Manoj, K., Golden, R.N., Hameed, H., Khalid, M.B., Emad, H.R.** Structural and Optical Properties of ZnO Thin film Prepared by Sol-gel Spin Coating *Materials Science-Poland* 38 2020: pp. 17 – 22. https://doi.org/10.2478/msp-2020-0016
18. **Heshmatpour, F., Aghakhanpour, R.B.** Synthesis and Characterization of Nanocrystalline Zirconia Powder by Simple Sol–gel Method with Glucose and Fructose as Organic Additives *Powder Technology* 205 2011: pp. 193 – 200. https://doi.org/10.1016/j.powtec.2010.09.011
19. **Balakrishnan, G., Sairam, T.N., Kuppusami, P., Thiumurugesan, R., Mohandas, E., Ganesan, V., Sastikumar, D.** Influence of Oxygen Partial Pressure on the Properties of Pulsed Laser Deposited Nanocrystalline Zirconia Thin Films *Applied Surface Science* 257 2011: pp. 8506 – 8510. https://doi.org/10.1016/j.apsusc.2011.05.003
20. **Mohammed, T., Maysoon, F.A.** Synthesis of ZnO-ZrO_2 Nanocomposites using Green Method for Medical Applications *International Journal of Modern Science* 10 2024: pp. 418e430. https://doi.org/10.33640/2405-609X.3366
21. **Ravi, D., Pitchaimani, V.** Microwave-assisted Hydrothermal Synthesis of ZnO@ZrO_2 Nanohybrid for Biomedical and Photocatalytic Applications *Colloids and Surfaces A: Physicochemical and Engineering Aspects* 688 2024: pp. 133574. https://doi.org/10.1016/j.colsurfa.2024.133574
22. **Sherly, E.D., Judith Vijaya, J., Clament Sagaya Selvam, N., John Kennedy, L.** Microwave Assisted Combustion Synthesis of Coupled ZnO–ZrO_2 Nanoparticles and Their role in the Photocatalytic Degradation of 2,4-dichlorophenol *Ceramics International* 40 2014: pp. 5681 – 5691. https://doi.org/10.1016/j.ceramint.2013.11.006
23. **Yixuan, W., Balakrishnan, G.** Microstructural, Antifungal and Photocatalytic Activity of NiO–ZnO Nanocomposite *Materials Science-Poland* 42 2024: pp. 1 – 9. https://doi.org/10.2478/msp-2023-0006
24. **Mohammed, A.W., Saad, M.Y., Walied, A.A.M., Hoda, R.G.** Remarkable Photocatalytic Activity of Zr doped ZnO and ZrO_2/ZnO Nanocomposites: Structural, Morphological and Photoluminescence Properties *Materials Chemistry and Physics* 256 2020: pp. 123754. https://doi.org/10.1016/j.matchemphys.2020.123754
25. **Wahba, M.A., Yakout, S.M**. Microwave Synthesized ZrO_2/ZnO Heterostructures: fast and High Charge Separation Solar Catalysts for Dyes-Waste Degradation *Journal of Sol-Gel Science and Technology* 104 2022: pp. 330 – 341. https://doi.org/10.1007/s10971-022-05936-4
26. **Abhijit, S.L., Abbas, S.P., Shivaji, V.B., Yogesh, V.H., Tukaram, R.G., Vijay, B.A., Sandesh, R.J., Sandeep, A.A.** Studies on Combustion Synthesized ZnO and ZnO@ZrO_2 Nanocomposites for Dye Contaminated Wastewater Treatment *Next Sustainability* 4 2024: pp. 100053. https://doi.org/10.1016/j.nxsust.2024.100053
27. **Długosz, O., Szostak, K., Banach, M.** Photocatalytic Properties of Zirconium Oxide–Zinc Oxide Nanoparticles Synthesised using Microwave Irradiation *Applied Nanoscience* 10 2020: pp. 941 – 954. https://doi.org/10.1007/s13204-019-01158-3

© Yuan et al. *2025* Open Access This article is distributed under the terms of the Creative Commons Attribution 4.0 International License (http://creativecommons.org/licenses/by/4.0/), which permits unrestricted use, distribution, and reproduction in any medium, provided you give appropriate credit to the original author(s) and the source, provide a link to the Creative Commons license, and indicate if changes were made.